A&A 554, A70 (2013)
DOI: 10.1051/0004-6361/201321651

Astronomy & Astrophysics

Herschel PEP/HerMES: the redshift evolution ($0 \leq z \leq 4$) of dust attenuation and of the total (UV+IR) star formation rate density⋆

D. Burgarella[1], V. Buat[1], C. Gruppioni[2], O. Cucciati[2], S. Heinis[1], S. Berta[3], M. Béthermin[4], J. Bock[5,6], A. Cooray[7,5], J. S. Dunlop[8], D. Farrah[9,10], A. Franceschini[11], E. Le Floc'h[4], D. Lutz[3], B. Magnelli[3], R. Nordon[3], S. J. Oliver[9], M. J. Page[12], P. Popesso[3], F. Pozzi[13], L. Riguccini[4], M. Vaccari[11,14], and M. Viero[5]

[1] Aix–Marseille Université, CNRS, LAM (Laboratoire d'Astrophysique de Marseille) UMR 7326, 13388 Marseille, France
e-mail: denis.burgarella@oamp.fr
[2] INAF–Osservatorio Astronomico di Bologna, via Ranzani 1, 40127 Bologna, Italy
[3] Max-Planck-Institut für Extraterrestrische Physik (MPE), Postfach 1312, 85741 Garching, Germany
[4] Laboratoire AIM-Paris-Saclay, CEA/DSM/Irfu – CNRS – Université Paris Diderot, CE-Saclay, pt courrier 131, 91191 Gif-sur-Yvette, France
[5] California Institute of Technology, 1200 E. California Blvd., Pasadena, CA 91125, USA
[6] Jet Propulsion Laboratory, 4800 Oak Grove Drive, Pasadena, CA 91109, USA
[7] Dept. of Physics & Astronomy, University of California, Irvine, CA 92697, USA
[8] Institute for Astronomy, University of Edinburgh, Royal Observatory, Blackford Hill, Edinburgh EH9 3HJ, UK
[9] Astronomy Centre, Dept. of Physics & Astronomy, University of Sussex, Brighton BN1 9QH, UK
[10] Department of Physics, Virginia Tech, Blacksburg, VA 24061, USA
[11] Dipartimento di Fisica e Astronomia, Università di Padova, vicolo Osservatorio, 3, 35122 Padova, Italy
[12] Mullard Space Science Laboratory, University College London, Holmbury St. Mary, Dorking, Surrey RH5 6NT, UK
[13] INAF – Osservatorio Astronomico di Roma, via di Frascati 33, 00040 Monte Porzio Catone, Italy
[14] Astrophysics Group, Physics Department, University of the Western Cape, Private Bag X17, 7535 Bellville, Cape Town, South Africa

Received 5 April 2013 / Accepted 29 April 2013

ABSTRACT

Using new homogeneous luminosity functions (LFs) in the far-ultraviolet (FUV) from VVDS and in the far-infrared (FIR) from *Herschel*/PEP and *Herschel*/HerMES, we studied the evolution of the dust attenuation with redshift. With this information, we were able to estimate the redshift evolution of the total (FUV + FIR) star formation rate density ($\mathrm{SFRD_{TOT}}$). By integrating $\mathrm{SFRD_{TOT}}$, we followed the mass building and analyzed the redshift evolution of the stellar mass density (SMD). This article aims at providing a complete view of star formation from the local Universe to $z \sim 4$ and, using assumptions on earlier star formation history, compares this evolution with previously published data in an attempt to draw a homogeneous picture of the global evolution of star formation in galaxies. Our main conclusions are that: 1) the dust attenuation A_{FUV} is found to increase from $z = 0$ to $z \sim 1.2$ and then starts to decrease until our last data point at $z = 3.6$; 2) the estimated SFRD confirms published results to $z \sim 2$. At $z > 2$, we observe either a plateau or a small increase up to $z \sim 3$ and then a likely decrease up to $z = 3.6$; 3) the peak of A_{FUV} is delayed with respect to the plateau of $\mathrm{SFRD_{TOT}}$ and a probable origin might be found in the evolution of the bright ends of the FUV and FIR LFs; 4) using assumptions (exponential rise and linear rise with time) for the evolution of the star formation density from $z = 3.6$ to $z_{\mathrm{form}} = 10$, we integrated $\mathrm{SFRD_{TOT}}$ and obtained a good agreement with the published SMDs.

Key words. early Universe – cosmology: observations – galaxies: star formation – infrared: galaxies – galaxies: starburst – ultraviolet: galaxies

1. Introduction

One of the main objectives in astrophysics during the past 15 years has been to follow the cosmic star formation rate density (SFRD) at ever earlier epochs. But whenever optical data are used, one must apply a dust correction to the luminosity densities (LDs) and a calibration into SFRDs (with their associated uncertainties) to obtain a relevant estimate. Knowing how the dust attenuation evolves in redshift is therefore mandatory if one wishes to study the redshift evolution of the SFRD.

For instance, Takeuchi et al. (2005) estimated the cosmic evolution of the SFRD from the far-ultraviolet (FUV) and far-infrared (FIR = bolometric IR). They found an increase of the fraction of hidden SFR from 56% locally to 84% at $z = 1$. The LDs show a significant evolution because the FIR LD evolves faster than the FUV. Their ratio $\rho_{\mathrm{FIR}}/\rho_{\mathrm{FUV}}$ increases from ~ 4 ($A_{\mathrm{FUV}} \sim 1.3$ mag) locally to $\sim$15 ($A_{\mathrm{FUV}} \sim 2.3$ mag) at $z = 1$. Cucciati et al. (2012) used the VIMOS-VLT Deep Survey to show from the FUV only that the mean dust attenuation A_{FUV} agrees with Takeuchi et al. (2005) over the range $0 < z < 1$. Then it remains at the same level to $z \sim 2$, and declines to ~ 1 mag at $z \sim 4$.

In this article, we use the FUV luminosity functions (LFs) published in Cucciati et al. (2012) from the VLT along with the FIR LFs from *Herschel*/PACS and SPIRE data[1] of a

⋆ *Herschel* is an ESA space observatory with science instruments provided by European-led Principal Investigator consortia and with important participation from NASA.

[1] From two *Herschel* large programmes: PACS evolutionary probe (PEP, Lutz et al. 2011) and the *Herschel* Multi-tiered Extragalactic Survey (HerMES, Oliver et al. 2012).

PACS-selected sample (Gruppioni et al. 2013) to constrain the redshift evolution of $\log_{10}(L_{\rm FIR}/L_{\rm FUV})$ (aka IRX) to $z \sim 4$ for the first time directly from FIR data. With this information, we can estimate the redshift evolution of $\rho_{\rm FIR}/\rho_{\rm FUV}$ as well as $\rho_{\rm TOT} = \rho_{\rm FIR} + \rho_{\rm FUV}$. Finally, by integrating $\rho_{\rm TOT}$, we estimate the cosmic evolution of the stellar mass density (SMD) with redshift.

Throughout this paper we adopt a ΛCDM cosmology with $(H_0, \Omega_{\rm m}, \Omega_\Lambda) = (70, 0.3, 0.7)$, where H_0 is in $\rm km\,s^{-1}\,Mpc^{-1}$. All SFR and stellar masses presented assume, or have been converted to, a Salpeter IMF.

2. Luminosity functions

Our analysis at $z \sim 0$ is based on the FUV LF from Wyder et al. (2005) and the FIR LF from Takeuchi et al. (2005), and for $0 < z < 4$ on the FUV LF from Cucciati et al. (2012) and the FIR LF from Gruppioni et al. (2013). In the FIR and at $z > 0$, the sample was selected in the PACS bands but used the full *Herschel*/PACS + *Herschel*/SPIRE SED data. The PACS selection means that we can miss sources toward the upper end of the redshift range. The LFs were evaluated from homogeneous datasets in the FUV and the FIR. This minimizes biases and keeps the same reference indicator throughout cosmic times with a simple well-defined and controlled selection function. This is one of the strengths of this work. The FUV LFs were not corrected for dust attenuation. We defined the LFs as a number density of galaxies with luminosity in logarithmic intervals, $[\log_{10} L, \log_{10} L + {\rm d}\log_{10} L]$, where $\Phi(L) = {\rm d}n/{\rm d}\log_{10} L$ and the luminosity is defined as $L \equiv \nu L_\nu$. FIR luminosities were defined as $\Phi(L) = \Phi_\star(\frac{L}{L_\star})^{1-\alpha} \exp(-\frac{1}{2\sigma^2}[\log_{10}(1 + \frac{L}{L_\star})]^2)$.

Observed uncertainties from Cucciati et al. (2012) and from Gruppioni et al. (2013) were used whenever available. However, some of the Schechter parameters were fixed when the LFs were derived, namely α for the FUV LFs and α plus σ for the FIR LFs. Both in FUV and in FIR, we assumed uncertainties of 10% up to $z = 1$, 20% up to $z = 2$ and 40% beyond for these fixed parameters. This level of uncertainty is similar to that of previous works in FUV (e.g. Oesch et al. 2010; van den Burg et al. 2010) and in FIR (Casey et al. 2012). We propagated uncertainties by simulating 2000 realizations drawn from 1σ Gaussian distributions for each parameter with known uncertainties and from a flat distribution (i.e., equiprobability) for the fixed ones. We assumed that all fixed values are equiprobable given the weak observational constraints. Finally, we interpolated the FUV and FIR Schechter parameters on the same redshift grid between $z = 0$ and $z = 3.6$.

Table 1 and Fig. 1 show the redshift variation of the LFs in FIR. The known difference in the FIR and FUV LFs (e.g. Takeuchi et al. 2005) are clearly illustrated here: bright FIR galaxies are more numerous than bright FUV galaxies at $\log_{10}(L[L_\odot]) > 10$. In the FUV, except in the highest redshift bins, $L^\star$ and $\Phi^\star$ remain approximately constant while the faint-end slope evolves. The FIR faint end slope is not observationally constrained at high z, and Gruppioni et al. (2013) fixed it to $\alpha = 1.2$. However, $L^\star$ and $\Phi^\star$ were allowed to change with redshift. These different evolutions of the FUV and FIR LFs are reflected in Fig. 1 and explain the evolution of the cosmic SFRD and dust attenuation.

3. Dust attenuation traced by the FIR-to-FUV LD ratio

Figure 2 presents the dust attenuation in the FUV vs. z and the ratio of the FIR-to-FUV LDs integrated in the range $\log_{10}(L[L_\odot]) = [7, 14]$ in the FUV (i.e. $L^{\rm min}_{\rm FUV} = 1.65 \times 10^{-4} L^\star_{z=3}$, Bouwens et al. 2009) and [8, 14] in the FIR. The FUV dust attenuation is estimated from the IRX and converted to $A_{\rm FUV}$ using Burgarella et al. (2005)[2]. The redshift evolution of $A_{\rm FUV}$ agrees with Cucciati et al. (2012). Note that Cucciati et al. (2012) estimated $A_{\rm FUV}$ through an analysis of individual SEDs up to

Table 1. Schechter parameter for FUV and FIR luminosity functions.

Redshift range	$M^\star$ or $L^{\star a}$	$\Phi_\star$	α	σ^b
FUV luminosity functions				
$0.0 < z < 0.1^c$	−18.04 ± 0.11	−2.370 ± 0.06	−1.22 ± 0.07	–
$0.05 < z < 0.2^d$	−18.12 ± 0.00	−2.155 ± 0.03	−1.05 ± 0.04	–
$0.2 < z < 0.4^d$	−18.3 ± 0.20	−2.161 ± 0.06	−1.17 ± 0.05	–
$0.4 < z < 0.6^d$	−18.4 ± 0.10	−2.180 ± 0.06	−1.07 ± 0.07	–
$0.6 < z < 0.8^d$	−18.3 ± 0.10	−2.021 ± 0.05	−0.90 ± 0.08	–
$0.8 < z < 1.0^d$	−18.7 ± 0.10	−2.045 ± 0.05	−0.85 ± 0.10	–
$1.0 < z < 1.2^d$	−19.0 ± 0.20	−2.129 ± 0.07	−0.91 ± 0.16	–
$1.2 < z < 1.7^d$	−19.6 ± 0.20	−2.387 ± 0.10	−1.09 ± 0.23	–
$1.7 < z < 2.5^d$	−20.4 ± 0.10	−2.472 ± 0.03	−1.30 ± −0.26	–
$2.5 < z < 3.5^d$	−21.4 ± 0.10	−3.066 ± 0.03	−1.50 ± −0.60	–
$3.5 < z < 4.5^d$	−22.2 ± 0.20	−3.959 ± 0.04	−1.73 ± −0.69	–
FIR luminosity functions				
$z = 0^e$	9.25 ± 0.00	−2.051 ± 0.00	1.23 ± 0.00	0.72 ± 0.00
$0.0 < z < 0.3^f$	10.12 ± 0.16	−2.29 ± 0.06	1.15 ± 0.05	0.52 ± 0.05
$0.3 < z < 0.45^f$	10.41± 0.03	−2.31 ± 0.03	1.2 ± −0.12	0.5 ± −0.05
$0.45 < z < 0.6^f$	10.55± 0.03	−2.35 ± 0.05	1.2 ± −0.12	0.5 ± −0.05
$0.6 < z < 0.8^f$	10.71 ± 0.03	−2.35 ± 0.06	1.2 ± −0.12	0.5 ± −0.05
$0.8 < z < 1.0^f$	10.97 ± 0.04	−2.40 ± 0.05	1.2 ± −0.12	0.5 ± −0.05
$1.0 < z < 1.2^f$	11.13 ± 0.04	−2.40 ± 0.05	1.2 ± −0.24	0.5 ± −0.10
$1.2 < z < 1.7^f$	11.37 ± 0.03	−2.70 ± 0.04	1.2 ± −0.24	0.5 ± −0.10
$1.7 < z < 2.0^f$	11.50 ± 0.03	−2.85 ± 0.03	1.2 ± −0.24	0.5 ± −0.10
$2.0 < z < 2.5^f$	11.60 ± 0.03	−3.01 ± 0.11	1.2 ± −0.48	0.5 ± −0.20
$2.5 < z < 3.0^f$	11.92 ± 0.08	−3.27 ± 0.18	1.2 ± −0.48	0.5 ± −0.20
$3.0 < z < 4.2^f$	11.90 ± 0.16	−3.74 ± 0.12	1.2 ± −0.48	0.5 ± −0.20

Notes. The top panel lists the FUV LFs, the bottom panel the FIR LFs. For all parameters with an uncertainty set to 0.00, we assumed a 20% or error. [(a)] $L^\star$ $[L_\odot]$ for FIR LFs or $M^\star$ [AB mag] for FUV LFs; [(b)] σ only needed for FIR LFs; [(c)] from Wyder et al. (2005); [(d)] from Takeuchi et al. (2005); [(e)] Cucciati et al. (2012); [(f)] Gruppioni et al. (2013).

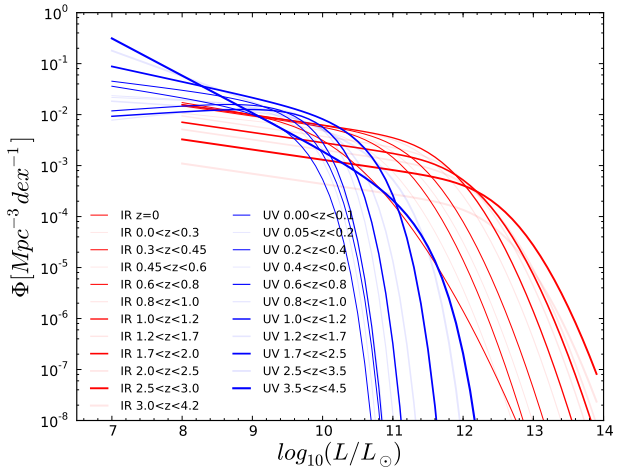

Fig. 1. Redshift evolution of the FIR (red, Gruppioni et al. 2013) and FUV (blue, Cucciati et al. 2012) LFs. Note that the FUV LFs are uncorrected for dust attenuation. The LFs at every other redshift are plotted in bold. The others are fainter to facilitate reading the figure. The LFs are plotted within the limits of integration.

[2] The conversion from IRX to $A_{\rm FUV}$ from Burgarella et al. (2005) is valid at $\log_{10}(L_{\rm FIR}/L_{\rm FUV}) > -1.2$: $A_{\rm FUV} = -0.028\,[\log_{10} L_{\rm FIR}/L_{\rm FUV}]^3 + 0.392[\log_{10} L_{\rm FIR}/L_{\rm FUV}]^2 + 1.094[\log_{10} L_{\rm FIR}/L_{\rm FUV}] + 0.546$.

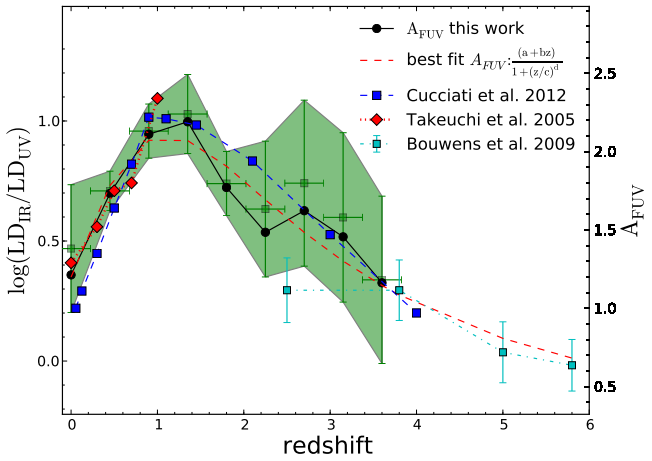

Fig. 2. Left axis: ratio of the FIR-to-FUV LDs (IRX). Right axis: FUV dust attenuation ($A_{\rm FUV}$). The red dotted line with red diamonds is taken from Takeuchi et al. (2005). The green filled area and green dots are the associated uncertainties estimated through bootstrapping with 2000 drawings. Black dots denote the values directly computed from the LFs. At $z = 3.6$, $A_{\rm FUV}$ reaches about the same value as at $z = 0$. Takeuchi et al. (2005) (red diamonds) used an approach identical to ours while an SED analysis (no FIR data) is performed in Cucciati et al. (2012) (blue boxes). Bouwens et al. (2009) are estimates based on the UV slope β. The limiting FUV luminosity is $10^7 L_\odot$ or $1.65 \times 10^{-4} L^\star_{z=3}$. The best fit is given by $A_{\rm FUV}(z) = \frac{(a+bz)}{1+(z/c)^d}$ with $a = 1.20$, $b = 1.50$, $c = 1.77$, and $d = 2.19$.

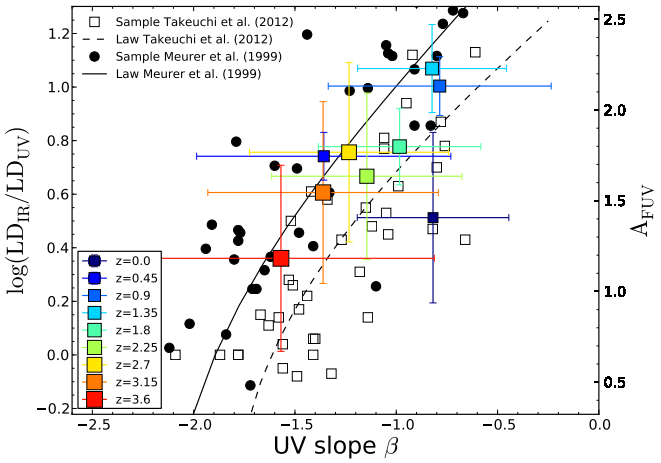

Fig. 3. Dust attenuation vs. redshift. The boxes are color-coded according to redshift. Note that the x-axis bars correspond to the dispersion in UV slope while the y-axis bars are evaluated from the uncertainties in the LFs. The black dots denote the original data points from Meurer et al. (1999) and the black curve plots the law of Meurer et al. (1999). The black dashed line and gray boxes denote the update (using the same apertures in FUV and in FIR) from Takeuchi et al. (2012). Strictly speaking, our points and those from Meurer et al. (1999) are not comparable because we used volume-corrected LFs and not individual galaxies as in Meurer et al. (1999). In the diagram, the color-coded points show an almost continuous decrease with increasing redshift and lie in between the Meurer et al. (1999) and Takeuchi et al. (2012) laws. We emphasize that the dust attenuation $A_{\rm FUV}$ is estimated from the IRX and not from the UV slope β.

$\lambda_{\rm obs} = 2.2$ μm (Ks-band). Figure 2 suggests a local minimum at $z \sim 2$ that might be caused by UV-faint galaxies (see Fig. 7 in Cucciati et al. 2012) that are responsible for a peak observed in the FUV LD that is not observed in the FIR. Since the fields observed in FUV and in FIR are not the same, another origin might be found in cosmic variance. The bottom line is that the existence of this trough in $A_{\rm FUV}$ seems dubious. Finally, higher redshift $A_{\rm FUV}$ from the UV slope, β, suggest a continuous decline at least to $z = 6$ (Bouwens et al. 2009).

We conclude that the cosmic dust attenuation $A_{\rm FUV}$ reaches an absolute maximum at $z \sim 1.2$ followed by a global decline to $z = 3.6$, where it reaches about the same level as measured at $z = 0$.

The β method is popular because it estimates the total SFR from the FUV only. This is most useful at high redshifts where the samples are UV-selected (see Burgarella et al. 2011; Bouwens et al. 2012; Heinis et al. 2013). We propose to follow the redshift evolution of the cosmic volume-averaged points in the IRX-β diagram (Fig. 3) to constrain models. However, we must caution that the values plotted in Fig. 3 cannot be directly compared with galaxies. The x-axis was calculated from the averaged rest-frame FUV – near-UV colors (e.g. Cortese et al. 2006). Horizontal error bars indicate the dispersion of the FUV slope. The IRX was estimated from LFs and is therefore volume-corrected. Vertical error bars are uncertainties. This IRX-β plot can be interpreted as the location of a comoving volume as a function of redshift. From $z \sim 1$ to $z \sim 4$, the points evolve downward parallel to the original law of Meurer et al. (1999) and the update reported in Takeuchi et al. (2012).

4. The total FUV+FIR star formation density and stellar mass density

The calibration from LD to SFRD is problematic (e.g. Kobayashi et al. 2013) in the FUV and also in the FIR (see discussions in Kennicutt 1998; Schaerer et al. 2013). In agreement with Casey et al. (2012), we used the Kennicutt (1998) calibrations and assumed a Salpeter initial mass function (IMF) to allow a better comparison with other published SFRDs. Note that the AGN contribution to the FIR LDs was estimated in FIR using an SED fitting and subtracted. It means that the presented FIR LD is due to star formation only.

Figure 4 suggests a flattening of the total SFRD up to $z \sim 3$ (as in Chary & Elbaz 2001; Perez-Gonzalez et al. 2005; Le Floc'h et al. 2005; Franceschini et al. 2010), where the UV data favor a peak followed by a decrease. Note that we cannot rule out a small increase or decrease within the uncertainties. The plateau up to $z \sim 2.5$ was reported in Rodighiero et al. (2010) and Magnelli et al. (2011), while the decrease of $\rho_{\rm SFR}$ at $z \geq 2.5$ was predicted in the Béthermin et al. (2012a) model based on the evolution of the mass function and sSFR estimated from LBGs. All in all, our total SFRD agrees fairly well with that of Hopkins & Beacom (2006) in the same redshift range. However, discrepancies exist: our total SFRD is lower at $z < 1$ and is only marginally consistent, but lower, at $z > 3$. Moreover, PACS data are less sensitive at higher than at lower redshift because the rest-frame wavelength moves into the mid-IR. The preliminary FIR SFRD from Vaccari et al. (in prep.; *Herschel*/SPIRE selection) agrees excellently over the $0 < z \leq 2$ range, but is slightly higher than that derived from PACS at $z > 3$. However, this is only a $\sim 2\sigma$ difference. Barger et al. (2012) published a FIR SFRD based on SCUBA-2 data that also agrees with ours at $2 < z < 4$. We first tried to fit $\rm SFRD_{TOT}$ with a one-peak analytical function (e.g. Hopkins & Beacom 2006; Behroozi et al. 2012), but the results are not satisfactory. So, we

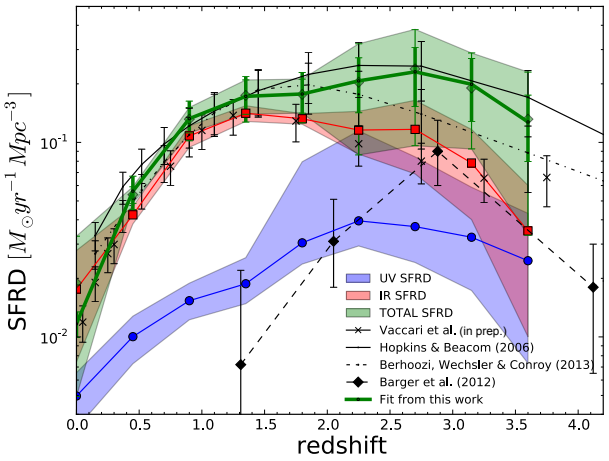

Fig. 4. SFRD densities in the FUV (blue), in the FIR (red), and in total (i.e., FUV + FIR) in green (other colors are due to overlaps of the previous colors). The lines are the mean values, while the lighter colors show the uncertainties evaluated from the 2000 runs as in Fig. 2. After the initial increase of the total SFRD from $z = 0$ to $z \sim 1.2$, it remains flat or slightly increases/decreases up to $z \sim 2.5$–3.0 followed by a decrease. Globally and over $0 < z \leq 3.6$, the total average SFRD is slightly below that reported in Hopkins & Beacom (2006) and agrees with that of Behroozi et al. (2012) up to $z \sim 2$. The SFRD from Barger et al. (2012) and preliminary results from *Herschel*/SPIRE estimated by Vaccari et al. (in prep.) agree with these trends. Symbols and lines are explained in the plot.

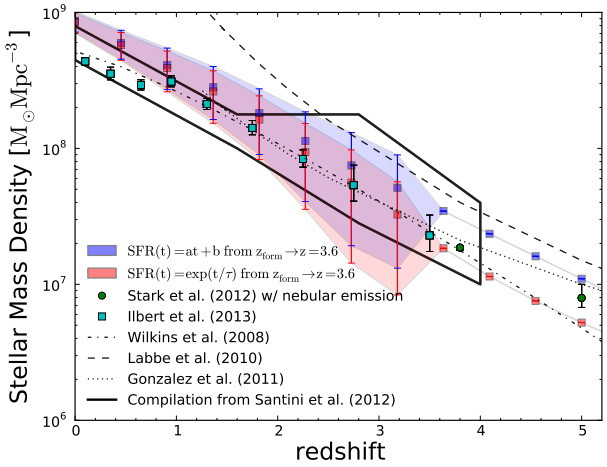

Fig. 5. Evolution of the cosmic SMD vs. redshift. The lines with blue and red boxes are the mean values evaluated by integration while the lighter colors show the uncertainties from the 2000 runs as in previous figures. We overplot the trends found in Labbe et al. (2010) at $z = 7$–8, Gonzalez et al. (2011) and Stark et al. (2013) at $3 < z < 7$. We also plot the line corresponding to the compilation of published measurements in Wilkins et al. (2008). Within the uncertainties, we find a good agreement of the SMD integrated from the SFRD with all other SMDs based on galaxy surveys from $z = 0.6$ to $z = 5$. The black-limited area represents the compilation of results in Santini et al. (2012). Scaled to the same cosmology and IMF (Salpeter). Using Gonzalez et al. (2011), we integrate down to luminosities equivalent to $M \sim 2500\ M_\odot$.

combined two Gaussians,

$$a_1 e^{\frac{-(z-z_1)^2}{2\sigma_1^2}} + a_2 e^{\frac{-(z-z_2)^2}{2\sigma_2^2}}, \quad (1)$$

with $a_1 = 0.1261 \pm 0.0222$, $\sigma_1 = 0.5135 \pm 0.0704$, $z_1 = 1.1390 \pm 0.0959$ and $a_2 = 0.2294 \pm 0.0222$, $\sigma_2 = 0.8160 \pm 0.0964$, $z_2 = 2.7151 \pm 0.0839$. At higher redshifts, we made assumptions that are explained below.

The cosmic SFRD presents a (weak) maximum at $z \sim 2.5$–3.0 (i.e., between 2.6–2.1 Gyr) while the dust attenuation presents a maximum at $z \sim 1.2$ (i.e. 5 Gyr). We tried to lock the faint-end slope of the UV LF to $\alpha = -1.2$, to see how far out in redshift the obscuration peak could potentially move, but we detected no change, suggesting this effect is solid. We have no definite explanation for this delay of ~2.7 Gyr. Type II supernovae start producing dust earlier than AGB stars (e.g. Fig. 3 in Valiante et al. 2009) but the difference in timescales is too short and only on the order of a few 10 Myr for the onset of dust formation. Dust grain destruction in the ISM might play a role (e.g. Dwek & Cherchneff 2011) but the efficiency of destruction is only poorly known and depends on the star formation history. These dust-related origins for the delayed maximum are un-likely. The best explanation might be that this delay is related to a global move of galaxies in the [$\log_{10}(L_{\rm FIR}/L_{\rm FUV})$ vs. $\log_{10}(L_{\rm FIR} + L_{\rm FUV})$] diagram. Buat et al. (2009) showed that galaxies evolve in redshift from $z = 0$ to $z = 2$ in this diagram, with high-redshift sources having lower IRX at given total luminosities. This change is very likely related to systematic changes of the FIR SEDs themselves (e.g. Elbaz et al. 2011; Nordon et al. 2012). This suggests that the shift might be caused by the relative importance of more luminous galaxies ($\log_{10} L_{\rm FUV}[L_\odot] \geq 10$) in the FUV as z evolves.

By integrating the SFRD, we can estimate the stellar-mass density (SMD; Fig. 5 and Table 2). To do this, we set the mass fraction of a generation of stars that is returned to the interstellar medium to a fixed value $R = 0.3$ (Fraternali & Tomassetti 2012). We also assumed a star formation history from $z = 3.6$ to the galaxy formation set at $z_{\rm form} = 10$. Option 1 is a linear extrapolation, while option 2 corresponds to a rising exponential $e^{t/\tau}$ with $\tau = 0.42$ (Papovich et al. 2011) that joins the observationally deduced SFRD[3].

Superimposed in Fig. 5 are recent SMDs (converted to Salpeter IMF if needed). Stark et al. (2013) accounted for the nebular emission line contribution to the broad-band fluxes used to infer stellar masses (see also Ono et al. 2010; de Barros et al. 2012). The trend from Labbe et al. (2010) lies above our points. The other SMDs agree within the uncertainties at $0.6 < z < 3.6$ for the two options described above. Wilkins et al. (2008) compiled measurements of the SMD from the literature and provided a best-fit parametric law $\rho_\star(z) = ae^{-bz^c}$ where $a = 0.0023$, $b = 0.68$ and $c = 1.2$. We also overplot this in Fig. 5. This curve slightly underestimates our SMD at very low redshifts, but follows the points derived from our data and our assumptions at higher redshifts.

We reach a fair agreement, especially at $0.6 < z < 3.6$. The discrepancy previously observed is reduced here, and is still marginally consistent at very low redshifts. As shown in Fig. 4, our total SFRD generally lies below that reported in Hopkins & Beacom (2006), suggesting that this previous evaluation of dust attenuation might be overestimated in this redshift range. The FIR data allowed us to reach a better agreement. Note that Hopkins & Beacom (2006) did not directly use MIR-based data to estimate their best-fitting parametric curve, but only to correct the obscuration of the FUV data.

Figure 6 shows the variation of the cosmic specific star formation rate (sSFR = SFRD/SMD) as a function of redshift.

[3] Selecting option 1 or 2 does have no impact on the results presented in Fig. 4.

Table 2. Evolution of the FUV and FIR LDs, the mean dust attenuation, and the cosmic SFRDs in FUV and FIR.

$z_{\rm mean}$	LD_{IR}/LD_{UV}	A_{FUV}[a] [mag]	$SFRD_{FUV}$[b] [10^{-2} $M_\odot$ yr^{-1} Mpc^{-3}]	$SFRD_{FIR}$[c] [10^{-2} $M_\odot$ yr^{-1} Mpc^{-3}]	$SFRD_{TOT}$[d] [10^{-2} $M_\odot$ yr^{-1} Mpc^{-3}]	$SFRD_{Hidden}$[e] fraction	β[f]
0.0	4.25 ± 3.25	1.38 ± 0.40	$0.50\,^{0.16}_{0.16}$	1.76 ± 1.02	1.86 ± 0.99	0.69 ± 0.10	–0.87 ± 0.37
0.45	7.11 ± 1.29	1.75 ± 0.13	$1.00\,^{0.28}_{0.28}$	4.24 ± 0.43	5.41 ± 0.54	0.82 ± 0.03	–1.41 ± 0.63
0.9	11.84 ± 2.75	2.14 ± 0.17	$1.54\,^{0.35}_{0.31}$	10.80 ± 1.37	13.10 ± 1.93	0.88 ± 0.03	–0.84 ± 0.55
1.35	13.44 ± 4.68	2.24 ± 0.25	$1.88\,^{0.68}_{0.39}$	14.13 ± 1.31	17.44 ± 3.39	0.89 ± 0.04	–0.87 ± 0.37
1.8	7.66 ± 2.40	1.80 ± 0.21	$3.05\,^{4.90}_{0.68}$	13.22 ± 0.83	17.70 ± 3.55	0.82 ± 0.04	–1.03 ± 0.40
2.25	6.03 ± 4.97	1.63 ± 0.45	$3.95\,^{7.51}_{1.02}$	11.58 ± 2.87	19.95 ± 11.73	0.74 ± 0.11	–1.20 ± 0.47
2.7	7.59 ± 6.99	1.79 ± 0.51	$3.69\,^{4.74}_{1.28}$	11.67 ± 4.78	24.03 ± 14.85	0.75 ± 0.15	–1.28 ± 0.49
3.15	5.54 ± 5.59	1.56 ± 0.52	$3.25\,^{2.63}_{1.52}$	7.83 ± 3.82	19.06 ± 10.28	0.68 ± 0.18	–1.41 ± 0.57
3.6	3.16 ± 3.55	1.19 ± 0.52	$2.46\,^{1.85}_{1.73}$	3.51 ± 2.51	12.84 ± 9.68	0.53 ± 0.23	–1.62 ± 0.76

Notes. SFR_{Hidden} corresponds to the percentage of SFRD in dust, $SFRD_{TOT}$ is the total (i.e., FUV + FIR) SFRD, and β is the mean slope estimated for the galaxies in the FUV sample. Lower integration limits are $L_{FUV}^{min} = 10^7\ L_\odot$ and $L_{FIR}^{min} = 10^8\ L_\odot$, upper limits are $L_{UV}^{max} = L_{FIR}^{max} = 10^{14} L_\odot$. [(a)] Calibrated from $\log_{10} LD_{IR}/LD_{UV}$ using Burgarella et al. (2005). Changing the integration limits to $\log_{10}(L[L_\odot]) = [4, 14]$ (resp. [9, 14]) in FUV and [5, 14] (resp. [10, 14]) in FIR would change A_{FUV} by <0.1 (resp. ∼−0.2) at $z \sim 3$–4 and <0.05 below $z < 2$. [(b)] Calibrated from LD_{UV} using Kennicutt (1998). [(c)] Calibrated from LD_{IR} using Kennicutt (1998). [(d)] Computed as $SFRD_{UV} + SFRD_{IR}$. Note that the values presented in this column are higher than $SFRD_{FUV} + SFRD_{FUV}$ from the two previous columns because they are the mean of the 2000 realizations estimated from the LFs, which happen to be above the sum of the SFRDs estimated by Cucciati et al. (2012) and Gruppioni et al. (2013). Changing the integration limits to $\log_{10}(L[L_\odot]) = [4, 14]$ (resp. [9, 14]) in FUV and [5, 14] (resp. [10, 14]) in FIR would change $SFRD_{TOT}$ by less than +8% (resp. –8%) at $z \leq 2.7$ but by + 56% and +158% at $z_{mean} = 3.15$ and $z_{mean} = 3.6$ (resp. –15% and –32%). [(e)] Computed as $SFRD_{UV}/SFRD_{IR}$. [(h)] This column presents the mean β only for the objects detected in the UV.

Previous observational results often suggested a flat evolution of the sSFR at $z > 2$ (e.g. Gonzalez et al. 2012; Bouwens et al. 2012; Schaerer et al. 2013), while most theoretical models predict a continuous rise (e.g. Bouche et al. 2010; Weinmann et al. 2011; Dave et al. 2011). Regardless of the hypothesis selected to extrapolate the observed SFRD beyond $z > 3.6$ to $z_{form} = 10$, our sSFRs remain consistent with an increase at low redshifts. The influence of the SFRD assumed at $z > 3.6$ is not noticeable within the uncertainties at $z < 3.6$. A comparison with the sSFR of galaxies from Noeske et al. (2007), Daddi et al. (2007), Wuyts et al. (2011), and Bouwens et al. (2012) in Fig. 6 suggests that the most massive galaxies ($\log_{10} M_\star = 10^{10.5}$–$10^{11}[M_\odot]$) agree with our sSFRs (we corrected the SMDs to $R = 0.3$ and applied a correction to the calibration of the SFR if necessary). Finally, we note that at higher redshifts, option 1 continues to rise while option 2 shows a flattening at $4 < z < 5$ followed by an increase at $z > 5$. We stress, though, that by assuming an exponential rise above $z > 4$ with a value of the time constant (τ = 420 Myr as in Papovich et al. 2011) and the formation of galaxies at $z_{form} = 10$ implies that the observed plateau at $4 < z < 5$ must be temporary. Changing τ and/or z_{form} to higher redshifts would shift the increase in sSFR to earlier times. Theoretically, fixing $z_{form} = \infty$ would translate into a flat sSFR.

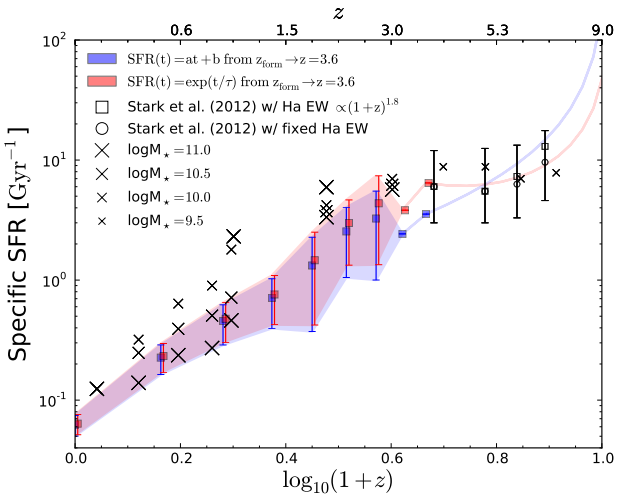

Fig. 6. Cosmic sSFR vs. z extrapolated beyond the observed limit at $z = 3.6$ with different options (see text). At $z < 4$, crosses are extracted from several galaxy surveys and are shown as a function of the considered $\log_{10} M_\star$ in Noeske et al. (2007), Daddi et al. (2007), and Wuyts et al. (2011) and at $z > 4$ in Bouwens et al. (2012). Below $z = 3.6$, our data suggest that the sSFR are dominated by $\log_{10} M_\star \sim 10.5$–$11.0$ galaxies. At $z > 4$ the extrapolations agree with $\log_{10} M_\star \sim 9.5$, as evaluated by Bouwens et al. (2012).

5. Discussion and conclusions

The variation of the cosmic dust attenuation with redshift as estimated from the IR to FUV luminosity ratio suggests a peak in the dust attenuation at $z \sim 1.2$ followed by a decline to $z = 3.6$. This result confirms the Cucciati et al. (2012) dust attenuation estimated from SED fitting without FIR data. Moreover, the redshift evolution of the volume-corrected IRX-β points globally follows the IRX-β law from $z = 0.4$ to $z = 3.6$.

The total (FUV+FIR) cosmic SFRD starts to decline above $z = 3$–4 and reaches the same level at $z \sim 5$–6 as is measured locally if we assume no variations in this trend. At $z = 3$–4, the decrease observed in the SFRD is not unexpected: most high-redshift studies clearly suggest such a trend through rest-frame UV observations (e.g. Hopkins & Beacom 2006; Bouwens et al. 2011) and predictions in Béthermin et al. (2012a). Backwards in time from today, this decline is preceded by a rise from $z \sim 0$ to a break at $z \sim 1$–2, followed by a plateau up to $z = 3$–4.

When we compare Fig. 2 with Fig. 4, the peak of the dust attenuation is delayed with respect to the plateau of the total

SFRD. It is also coeval with the final decrease at $z = 1$–1.5, the peak of the less luminous AGNs (Hopkins 2007. A similar peak seems to appear at $z = 1$–2 (depending on the stellar mass) of the cosmological merger rate (Conselice et al. 2008) and of the CIB Béthermin et al. (2012b). Are all these effects related to the same physical phenomena, and if so, what are their characteristic timescales? To better understand the delay, it is necessary to perform an analysis via models that are fed with data of the gas content and the metallicity evolution.

Using the observed cosmic SFRD along with the assumption of an exponential rise from $z_{\rm form} = 10$ to $z = 3.6$, we were able to recover the SMD evaluated from galaxy surveys. With the same assumption, we predict a flattening of the sSFR at $3 < z < 5$ followed by a new steepening at $z > 5$.

Figures 2 and 4 taken together at face value would suggest that the universe's dusty era (meaning dust attenuation higher than in the local universe) started at $z = 3$–4 simultaneously with the rise of a universe-wide star-formation event.

Figures 4–6 allowed us to follow the SFRD, the SMD, and the sSFR over most of the Hubble time in a consistent way. However, large uncertainties prevented us from closing the case. Additionaly, it remains quite puzzling that GRB-based analyses suggest a much shallower decrease (Kistler et al. 2009; Robertson & Ellis 2012) than Lyman-break galaxies. The statistical significance of these results is still debated because of the low number of objects at high redshifts and a possible modification of the IMF (Dwek & Cherchneff 2011; Hayward et al. 2013). Another possibility is that GRBs might still be biased toward certain types of star-forming galaxies, even though this bias may be lower than thought a few years ago.

Acknowledgements. PACS has been developed by a consortium of institutes led by MPE (Germany) and including UVIE (Austria); KU Leuven, CSL, IMEC (Belgium); CEA, LAM (France); MPIA (Germany); INAF-IFSI/OAA/OAP/OAT, LENS, SISSA (Italy); IAC (Spain). This development has been supported by the funding agencies BMVIT (Austria), ESA-PRODEX (Belgium), CEA/CNES (France), DLR (Germany), ASI/INAF (Italy), and CICYT/MCYT (Spain). SPIRE has been developed by a consortium of institutes led by Cardiff Univ. (UK) and including: Univ. Lethbridge (Canada); NAOC (China); CEA, LAM (France); IFSI, Univ. Padua (Italy); IAC (Spain); Stockholm Observatory (Sweden); Imperial College London, RAL, UCL-MSSL, UKATC, Univ. Sussex (UK); and Caltech, JPL, NHSC, Univ. Colorado (USA). This development has been supported by national funding agencies: CSA (Canada); NAOC (China); CEA, CNES, CNRS (France); ASI (Italy); MCINN (Spain); SNSB (Sweden); STFC, UKSA (UK); and NASA (USA). The authors acknowledge financial contribution from the contracts PRIN-INAF 1.06.09.05 and ASI-INAF I00507/1 and I005110. SPIRE has been developed by a consortium of institutes led by Cardiff University (UK) and including University of Lethbridge (Canada); NAOC (China); CEA, OAMP (France); IFSI, University of Padua (Italy); IAC (Spain); Stockholm Observatory (Sweden); Imperial College London, RAL, UCL-MSSL, UKATC, University of Sussex (UK); and Caltech/ JPL, IPAC, University of Colorado (USA). This development has been supported by national funding agencies: CSA (Canada); NAOC (China); CEA, CNES, CNRS (France); ASI (Italy); MCINN (Spain); Stockholm Observatory (Sweden); STFC (UK); and NASA (USA). The data presented in this paper will be released through the *Herschel* Database in Marseille (HeDaM; http://hedam.oamp.fr/HerMES). This work makes use of TOPCAT (http://www.star.bristol.ac.uk/?mbt/topcat/).

References

Barger, A. J., Wang, W. H., Cowie, L. L., et al. 2012, ApJ, 761, 89
Behroozi, P. S., Wechsler, R. S, & Conroy, C. 2012, ApJ, submitted [arXiv:1207.6105]
Béthermin, M., Le Floc'h, E., Ilbert, O., et al. 2012a, A&A, 542, A48
Béthermin, M., Daddi, E., Magdis, G., et al. 2012b, ApJ, 757, L23
Bouché, N., Dekel, A., Genzel, R., et al. 2010, ApJ, 718, 1001
Bouwens, R. J., Illingworth, G. D., Franx, M., et al. 2009, ApJ, 705, 936
Bouwens, R. J., Illingworth, G. D., Oesch, P. A., et al. 2011, ApJ, 737, 90
Bouwens, R. J., Illingworth, G. D., Oesch, P. A., et al. 2012, ApJ, 754, 83
Buat, V., Takeuchi, T. T., Burgarella, D., et al. 2009, A&A, 507, 693
Burgarella, D., Buat, V., & Iglesias-Páramo, J. 2005, MNRAS, 360, 1413
Burgarella, D., Heinis, S., Magdis, G., et al. 2011, ApJ, 734, L12
Casey, C. M., Berta, S., Bethermin, M., et al. 2012, ApJ, 761, 140
Chary, R., & Elbaz, D. 2001, ApJ, 556, 562
Conselice, C. J., Rajgor, S., Myers, R., et al. 2008, MNRAS, 386, 909
Cortese, L., Boselli, A., Buat, V., et al. 2006, ApJ, 637, 242
Cucciati, O., Tresse, L., Ilbert, O., et al. 2012, A&A, 539, A31
Daddi, E., Dickinson, M., Morrison, et al. 2007, ApJ, 670, 156
Davé, R., Oppenheimer, B. D., & Finlator, K. 2011, MNRAS, 415, 11
de Barros, S., Schaerer, D., & Stark, D. P. 2012 [arXiv:1207.3663]
Dwek, E., & Cherchneff, I. 2011, ApJ, 727, 63
Elbaz, D., Dickinson, M., Hwang, H. S., et al. 2011, A&A, 533, A119
Franceschini, A., Rodighiero, G., Vaccari, M., et al. 2010, A&A, 517, A74
Fraternali, F., & Tomassetti, M. 2012, MNRAS, 426, 2166
Gruppioni, C., Pozzi, F., Rodighiero, G., et al. 2013, MNRAS, 432, 23
González, A., Labbé, I., & Bouwens, R. J. 2011, ApJ, 735, L34
Gonzàlez, A., Bouwens, R. J., Illingworth, G., et al. 2012, ApJ, submitted [arXiv:1208.4362]
Hayward, C. C., Narayanan, D., Keres, D., et al. 2013, MNRAS, 428, 2528
Heinis, S., Buat, V., Béthermin, et al. 2013, MNRAS, 429, 1113
Hopkins, A. M., & Beacom, J. F. 2006, ApJ, 651, 142
Hopkins, P. F., Richards, G. T., & Hernquist, L. 2007, ApJ, 654, 731
Ilbert, O., McCracken, H. J., & Le Fèvre, 0. 2013, A&A, submitted [arXiv:1301.3157]
Kennicutt, R. C. 1998, ARA&A, 36, 189
Kistler M. D., Yuksel, H., Beacom, J. F., et al. 2009, ApJ, 705, L104
Kobayashi, Masakazu, A. R., Inoue, Y., & Inoue, A. K. 2012, ApJ, 763, 3
Labbé, I., González, V., Bouwens, R. J., et al. 2010, ApJ, 716, L103
Le Floc'h, E., Aussel, H., Combes, F., et al. 2005, ApJ, 632, L169
Lutz, D., Poglitsch, A., Altieri, B., et al. 2011, A&A, 523, L90
Magnelli, B, Elbaz, D., Chary, R. R., et al. 2011, A&A, 528, A35
Meurer, G. R., Heckman, T. M., & Calzetti, D. 1999, ApJ, 521, 64
Noeske, K. G., Faber, S. M., Weiner, B. J., et al. 2007, ApJ, 660, L47
Nordon, R., Lutz, D., Genzel, R., et al. 2012, ApJ, 745, 192
Oesch, P. A., Bouwens, R. J., Carollo, C. M., et al. 2010, ApJ, 725, L150
Ono, Y., Ouchi, M., Shimasaku, K., et al. 2010, ApJ, 724, 1524
Oliver, S. J., Bock, J., Altieri, B., et al. 2012, MNRAS, 424, 1641
Papovich, C., Finkelstein, S. L., Ferguson, H. C., et al. 2011, MNRAS, 412, 1123
Pérez-González, P. G., Rieke, G. H., Le Floc'h, E., et al. 2005, ApJ, 630, 82
Robertson B. E., & Ellis, R. S. 2012, ApJ 744, 95
Rodighiero, G., Vaccari, M., Franceschini, A., et al. 2010, A&A, 515, A8
Santini, P., Fontana, A., Grazian, A., et al. 2012, A&A, 538, A33
Schaerer, D., de Barros, S., & Sklias, P. 2013, A&A, 549, A4
Stark, D. P., Schenker, M. A., Ellis, R. S., et al. 2013, ApJ, 763, 129
Takeuchi, T. T., Buat, V., & Burgarella, D. 2005, A&A, 440, L17
Takeuchi, T. T., Yuan, F., Ikeyama, A., et al. 2012, ApJ, 755, 144
Valiante, R., Schneider, R., Bianchi, S., et al. 2009, MNRAS, 397, 1661
Van den Burg, R. F. J., Hildebrandt, H., & Erben, T. 2010, A&A, 523, A74
Weinmann, S. M., Neistein, E., & Dekel, A. 2011, MNRAS, 417, 2737
Wilkins, S. M., Trentham, N., & Hopkins, A. M. 2008, MNRAS, 385, 687
Wuyts, S., Forster Schreiber, N. M., van der Wel, A., et al. 2011, ApJ, 742, 96
Wyder, T. K., Treyer, M. A., Milliard, B., et al. 2005, ApJ, 619, 15